Nanopore sculpting with noble gas ions

Share Your Story

Nanopore sculpting with noble gas ions

Qun Cai[a)],
Department of Physics, University of Arkansas, Fayetteville, Arkansas 72701, USA

Brad Ledden,
Department of Physics, University of Arkansas, Fayetteville, Arkansas 72701, USA

Eric Krueger,
Department of Physics, University of Arkansas, Fayetteville, Arkansas 72701, USA

Jene A. Golovchenko, and
Department of Physics, Harvard University, Cambridge, Massachusetts 02138, USA

Jiali Li[b)]
Department of Physics, University of Arkansas, Fayetteville, Arkansas 72701, USA

Abstract

We demonstrate that 3 keV ion beams, formed from the common noble gasses, He, Ne, Ar, Kr, and Xe, can controllably "sculpt" nanometer scale pores in silicon nitride films. Single nanometer control of structural dimensions in nanopores can be achieved with all ion species despite a very wide range of sputtering yields and surface energy depositions. Heavy ions shrink pores more efficiently and make thinner pores than lighter ions. The dynamics of nanopore closing is reported for each ion species and the results are fitted to an adatom diffusion model with excellent success. We also present an experimental method for profiling the thickness of the local membrane around the nanopore based on low temperature sputtering and data is presented that provides quantitative measurements of the thickness and its dependence on ion beam species.

Introduction

Recently we reported that a low energy Ar^+ ion beam could "sculpt" nanometer scale pores in silicon nitride and silicon dioxide films [1,2]. The Ar^+ ion beam incident on these solid membranes was shown to induce lateral mass transport on the surface of a membrane containing a prefabricated ~100 nm pore extending through its thickness. The transport was discovered by observing the continuous closing of this pore down to nanometer diameters during Ar^+ ion beam exposure. The utility of the method for creating single digit solid state nanopore single molecule detectors has been demonstrated [3-5]. Other methods of nanopore formation are also being actively explored [6]. The physics responsible for the ion beam sculpting process appears to be consistent with an adatom diffusion model [1,7,8]. However, another approach based on the notion of stimulated viscous flow has been advanced to account for the potentially related phenomena of ion beam induced ripple formation [9-11], and it must be admitted that the explanation for the ion sculpting phenomena may yet to be fully elucidated.

Low energy noble gas ion beams have been applied as an effective tool to modify surface structures and properties on various materials at the nanoscale [7-9,12-15]. Here we present

---

[b)] Correspondence author's: jialili@uark.edu.
[a)] Current address: Surface Physics Laboratory, Fudan University, Shanghai, China

ion beam sculpting results for a variety of noble gas ions and ion beam fluxes to drastically change some of the potentially relevant parameters of the process. We also introduce a method for thickness profiling the material near a nanopore and show that these profiles can be very sensitive to the nanopore forming ion beam species used.

Experimental methods and results

Samples with a single large (~100 nm diameter) hole were prefabricated in 30 μm × 30 μm free standing silicon nitride membranes supported on 380 μm (100) silicon substrates. The 275 nm thick, low stress (~200 MPa tensile) silicon nitride membranes were grown by low pressure chemical vapor deposition at the Cornell Nanofabrication Center. Photolithography and anisotropic wet KOH etching of silicon were used to create the free standing membranes. The initial large 0.1 μm diameter holes were created at the membrane's center using a focused ion beam (FIB, Micrion 9500) machine. The sizes of the all FIB holes were then determined by Transmission Electron Microscopy (TEM). To create 1-10 nanometer pores from the larger FIB holes, the samples were then "ion-sculpted" using a several hundred micron diameter 3 keV noble ion beam in an apparatus described below.

As illustrated in Fig.1 (a) and (b), the apparatus counts the ions transmitted through the hole in the silicon nitride membrane with a Channeltron single ion detector during the ion beam sculpting process. The ion counting rate instantly provides information about ion irradiation flux and the size of the hole as a function of time. During ion beam sculpting, a 50 eV electron beam irradiates the membranes to maintain surface charge neutrality. The apparatus is housed in a high-vacuum chamber (10^{-9} to 10^{-10} mbar) and the presence of the inert gases is verified by a residual gas analyzer. The comprehensive descriptions of the feedback-controlled ion beam sculpting apparatus can be found in our previous work [1, 16]. The apparatus also controls parameters such as sample temperature, ion beam flux, F, in ions $nm^{-2}s^{-1}$, and the time intervals that the ion beam can be switched on and off the sample. After the initial closing of a pore as indicated schematically in Fig.1b, the area of the pore can actually be made to increase or decrease during the exposure by adjusting these parameters [1, 16].

Figure 2a shows pores whose areas are decreasing as a function of time (and dose) for room temperature (28 °C) samples continuously irradiated by 3 keV He, Ne, Ar, Kr, and Xe ions at fluxes of 0.5-0.6 ions $nm^{-2}s^{-1}$. The pore area decreases at a rate that depends on the ion species. The heavier ions close the pore more quickly than lighter ions. The curvature of the closing traces in Figure 2(a) is concave up. When observed in the TEM the nanopore membranes made by lighter ions, He^+ and Ne^+, have less contrast and show fine grained microstructure (Fig.2b, He pore) whereas the nanopores made by heavier ions: Ar, Kr, and Xe, have higher contrast and show coarser grain microstructure (Fig.2b, Kr pore). When the ion beam flux is increased the efficiency of closing the pore on a per ion basis decreases. At fluxes lower than ~1 ion/(nm^2s), all the closing traces are concave up as in Fig.2a. However, when ion beam flux is increased, the closing traces are concave down as show in Fig. 2c for He at F=18 ions/nm^2/s and Kr at F=16.2 ions/nm^2/s. Keeping all the parameters the same as those in Fig.2a, but cooling the samples to -100 °C causes nearly closed nanopores to increase in size. Fig. 2d shows such openings for He, Ne, and Kr at F~0.5 ions/(nm^2s).

Figures 3a and 3b show pore area closing dynamics as a function of the total ion dose deposited in silicon nitride per nm^2 for He^+ and Kr^+ respectively. Heavy Kr ions close pores more efficiently than the lighter He ions. Fig.3d shows the stopping range of ions (He^+ and Kr^+) at 3 keV into the low stress silicon nitride film predicted by the computer simulation program SRIM (The Stopping and Range of Ions in Matter) [17].

Figure 2d suggests that whatever the mass transport mechanism responsible for the closing of nanopores by ion beam sculpting, it is negligible at low temperature where the sputter removal of surface material is dominant. This provides a means to measure the thickness profile of material that has been previously grown by the ion sculpting process at room temperature. Thus samples with prefabricated ~100 nm holes were first closed completely and then the ion beam was kept on the sample for 3 more seconds for each gas at 3 keV with fluxes of ~0.5 ions/(nm^2 sec). These samples were then cooled to -100°C and exposed to an Ar$^+$ beam at an energy of 3keV with a flux of ~0.5 ions/(nm^2 sec). At this temperature, the sputtering erosion effect dominates so the closed pores will open as shown in Fig.4a for He$^+$ and 4c for Kr$^+$ closed pores. The ion beam irradiation was stopped when the opening pore was approximately the size of the original prefabricated FIB hole. The exact flux of the Ar$^+$ ion beam used to open a pore was calculated by measuring the open pore area from a TEM image. The thickness of the center of the closed pore (the thinnest part) H_0 was then determined from a simplified relation from Klaus Wittmaack [18]: $H_0 = Y_s \Omega F t_0$, here t_0 is the time measured for opening the thinnest part of the closed pore, Ω is the atomic volume (~0.01 nm^3/atom) for Si or N, and Y_s is the sputtering yield of Ar$^+$ at 3 keV on $Si_{3.5}N_4$. The value of $Y_s = 2.06$ for Ar$^+$ at 3 keV is used and it is calculated from the simulation program SRIM (See table I). The sputtering yield Y_s for Ar, together with He in table I were also verified by measuring the time needed to sputter the entire 275 nm free standing membrane away. The measured Y_s value for He is 10 times smaller than Kr, consistent with the estimation from TRIM (Table I). For all pores completely closed by various gases, a total of 3 samples for each gas, the measured mean thickness H_0 is from 7 to 20 nm (see Table I). These average thickness values correlate with the ion penetration ranges for He, Ne, Ar, Kr, and Xe calculated from SRIM. The lighter ions have a larger penetration depth, as shown in Fig.3d for He, and make thicker nanopores. The estimated thickness of He$^+$ closed membrane is $H_0(He) = 19.6 \pm 2.5$ nm. Heavy ions have a smaller penetration depth, as shown in Fig. 3d for Kr, and make thinner pores: $H_0(Kr) = 9.9 \pm 0.9$ nm.

As the pore opens we assume the thickness H at the pore boundary changes with the pore radius R as:

$$H(t) = (H_0 + C_1 R^2(t) + C_2 R(t)) = Y_s \Omega F t \tag{1}$$

C_1 and C_2 are fitting parameters characterizing the thickness profile. Determining the pore radius R(t) from the opening pore area data in 4a and 4c ($A = \pi R^2(t)$), the thickness profiles of He$^+$ closed pore (Fig.4b) and a Kr$^+$ closed pore (Fig. 4d) were deduced from Equation 1. The thickness H_0 varies with ion species and ion beam parameters. For example, a Kr$^+$ pore closed at F=0.53 ions/(nm^2 sec) shown in Fig. 4d, is flat for R<20 nm. For a He$^+$ pore closed with F=0.58 ions/(nm^2 sec), the thickness profile is also flat for R<20 nm, as shown in Fig. 4b, although the He$^+$ pore is nearly twice as thick.

Analysis

Noble gas atoms of He, Ne, Ar, Kr, and Xe have atomic masses of 4, 20, 40, 84 and 131 AMU respectively. Differences in penetration depths, sputtering erosion rates, mass transport and morphological change are to be expected when these ions are accelerated to the same kinetic energy and then strike on a silicon nitride surface. From the computer simulation program SRIM, one can estimate sputtering parameters of various noble gas ions at 3 keV. The results are listed in Table I. These results show that the nuclear stopping power (the 3rd column) is the dominant mechanism determining ion range for all gasses except Helium. The penetration range for Helium ions is at least four times larger than the

other ions. Note how the heavier ions such as Ar^+, Kr^+, and Xe^+ deposit a large percentage of their energy in the top 5 nm of material.

To explain the pore closing ion beam sculpting results described above, an ion beam incident on a solid surface must clearly be capable of inducing lateral mass transport near the surface, resulting in the inward growth of a thin film from a prefabricated FIB hole boundary. Under some conditions, a nanopore or completely closed pore can also be opened into a big pore as demonstrated in Fig. 2d, 4a, 4c. This indicates that the model must also accommodate material removal through the sputtering process. Here we adopt the phenomenological model presented in reference [1] where the competition between lateral mass flow into the pore and ion sputter erosion of the pore determines the final net pore area changing rate. The opening of a pore is the result of ion sputter erosion of the pore edge, assumed to be ever present and temperature independent. The shrinking of a pore is a complicated process, and all the mechanisms have yet to be totally clarified. If we assume the lateral mass flowing into the pore is the result of the adatom surface diffusion as in references [1,2], then a quantitative relation for the pore area changing rate can be deduced as: Pore area changing rate= - pore area shrinking rate + pore opening rate:

$$\frac{\partial A}{\partial t} = \frac{\partial}{\partial t}\left(\pi R^2\right) = \frac{2\pi\Omega RF}{H}\left(-Y_a X_m \frac{K_1\left(\frac{R}{X_m}\right)}{K_0\left(\frac{R}{X_m}\right)} + S_E\right)$$

(2)

Where S_E is the effective cross section for sputter-erosion from the pore edge, H is the thickness of the film formed by filling in the nanopore, Ω is the atomic volume (~0.01 nm^3/ atom) for Si or N, F is the ion beam flux, X_m is the mean travel distance for adatoms, R is the radius of the pore, and K_0 and K_1 are modified Bessel functions of the second kind. Y_a is the mobile species or adatom generating yield on the surface. Here the adatom generating yield was calculated as the surface mobile atoms with kinetic energy less than the surface binding energy of 3.4 eV by the SRIM program as shown in Table I. All the solid curves in Fig.2a, 2c, 3a, and 3b are fits to the measured pore area as a function of time using equation 2.

To determine S_E, nanopore opening data in Fig.2d are used to fit Eq.2 assuming the closing term (first in brackets) is zero (i.e., the diffusion contribution to pore shrinking is presumably frozen out). S_E values obtained this way for He, Ne, Ar, Kr, and Xe ions are 11.3, 31.1, 47.2, 62.4, and 52.6 nm/ion respectively (also see in Table I). These S_E values are then used to fit data in Fig.2a. The X_m values obtained from these curve fittings are 430(He), 120(Ne), 96(Ar), 96(Kr), and 152(Xe) nm. Pore closing data was fitted to Eq.2 and X_m values were extracted for all He and Kr ions. Fig.3c shows plots of $1/X_m^2$ as a function of flux F for He and Kr. From the slope of $1/X_m^2$ versus flux, the diffusion constants of adatoms can be estimated [1]. For He ion sculpting process, the adatom diffusion constant is $1.1\pm0.2 \times 10^4$ nm^2/s; for Kr it's $1.2\pm0.1 \times 10^3$ nm^2/s.

The concave down high flux closing data in Fig.2c cannot be fitted to Eq.2 if the thickness of the filling in membrane is assumed to be a constant. However such behavior can be accommodated by the model if it is assumed that the growing membrane thickness decreases as the pore closes. The solid curves are the fitting results assuming the thickness H decreases linearly as the radius of the pore decreases. Predicting membrane thickness and profile is currently beyond the capabilities of any reasonably motivated model of which we are aware. Within the adatom diffusion picture discussed above membrane thickness is a parameter we have obtained from experimental measurements. In a more comprehensive model capable of predicting the membrane thickness, the competing roles of Y_a and S_E must surely play a

role. Thus like the pore formation itself the membrane thickness is being controlled by the competing thickness enhancing mobile atoms drawn to the pore region of the membrane, whose number is controlled by Y_a and X_m, and the thickness decreasing function of sputter erosion controlled by the sputtering yield Y_s (which must be closely related to S_E). Increased membrane thickness with the mean ion penetration depth suggests that the generation of mobile matter is not only on top of the surface, especially for He closed pores. The mobile matter is generated and contributes to the pore closing in the penetration range of the incident ions.

Another view can potentially also explain the mobile matter generated to account for the pore-closing phenomenon. In this view, the energy and matter deposited by the ion beam may create a very thin (~5 nm) stressed viscous surface layer. Due to ion implantation effects or surface tension, driven by a reduced viscosity and /or enhanced stress, the surface layer would relax, causing the pore to close. A related model has been used to explain atomic transport in sputter-induced rippling [9-11]. However, a concrete mathematical model has not been developed to quantitatively explain the pore closing phenomena by this mechanism.

The phenomenological diffusion model used in this work contains idealizations and assumptions connected with our lack of knowledge of many microscopic properties of matter under ion beam exposure; however the model qualitatively explains the experimental results, especially in predicting pore shrinking rate. It does not rule out the possibility that ion induced viscous flow can account for all or some of the mass transport. However, a comprehensive fluid mechanical model that can explain pore closing based on near surface ion beam deposition has yet to be fully articulated theoretically.

Summary

In this work we report experimental results and analysis for ion beam sculpting silicon nitride nanopore with different noble gas ions. Our experiments show that 3keV Helium, Neon, Argon, Krypton, and Xenon ion beams can be used to controllably "sculpt" nanoscale pores in silicon nitride films using a feedback controlled ion beam sculpting apparatus and demonstrates that strong variations in ion mass, flux and sample temperature can dramatically influence the pore diameters and membrane thickness profiles of the nanopores formed. We find that: (1) all the noble gas ion beams enable single nanometer control of structural dimensions in nanopores. (2) Every ion species above shows similar ion beam flux dependence of nanopore formation: as flux increases, the process of shrinking pores becomes less efficient. (3) At low flux, lighter ions are less efficient in closing nanopores. (4) The thickness and thickness profile of nanopores sculpted with different noble gas ion beam can be estimated by assuming that only sputter removal of surface material takes place at low temperature, from which we find that at low flux lighter ions make thicker nanopores. Computer simulations (SRIM and TRIM) and an "adatom" surface diffusion model are employed to explain the dynamics of nanopore dimension change by competing sputter erosion and surface mass transport processes induced by ion beam irradiation. These experiments reveal surface atomic transport phenomena and parameters that can be extracted for an adatom diffusion model in a quantitative way. On average, adatom travel distances are on the order of 10^2 nm.

Acknowledgments

References

1. Li J, Stein D, McMullan C, Branton D, Aziz MJ, Golovchenko JA. Ion-beam sculpting at nanometre length scales. Nature 2001;412(12 July):166–169. [PubMed: 11449268]

2. Stein D, Li J, Golovchenko JA. Ion-Beam Sculpting Time Scales. Physical Review Letters 2002;89(27)

3. Li J, Gershow M, Stein D, Brandin E, Golovchenko JA. DNA Molecules and Configurations in a Solid-state Nanopore Microscope. Nature Materials 2003;2:611–615.

4. Chen P, Gu J, Brandin E, Kim YR, Wang Q, Branton D. Probing Single DNA Molecule Transport Using Fabricated Nanopores. Nano Letters 2004;4(11):2293–8.

5. Fologea D, Gershow M, Ledden B, McNabb DS, Golovchenko JA, Li J. Detecting Single Stranded DNA with a Solid State Nanopore. Nano Letters 2005;5(10):1905–1909. [PubMed: 16218707]

6. Storm AJ, Chen JH, Ling XS, Zandbergen HW, Dekker C. Fabrication of solid-state nanopores with single-nanometre precision. Nature Materials 2003;2:537–540.

7. Erlebacher J, Aziz MJ, Chason E, Sinclair MB, Floro JA. Spontaneous pattern formation on ion bombarded Si(001). Phys Rev Lett 1999;82(11):2330–2333.

8. Erlebacher J, Aziz MJ, Chason E, Aziz MJ. Nonlinear amplitude evolution during spontaneous patterning of ion-bombarded Si(001). J Vac Sci Technol A 2000;18((1)(Jan/Feb)):115–120.

9. Mayer TM, Chason E, Howard AJ. Roughening instability and ion-induced viscous relaxation of SiO_2 surfaces. J Appl Phys 1994;76(3):1633–1643.

10. Carter G. Viscoelastic buckling and plastic -flow deterministic mechanistic mechanisms for ripple initiation on ion bombarded amorphous solids. Surface and Interface Analysis 1997;25:952–4.

11. Brongersma ML, Snoeks E, v Dillen T, Polman A. Origin of MeV ion irradiation-induced stress changes in SiO_2. J Appl Phys 2000;88(1):59–64.

12. Dubner AD, Wagner A, Melngailis J, Thompson CV. The role of the ion-solid interaction in ion-beam-induced deposition of gold. J Appl Phys 1991;70(2):665–673.

13. McLaren MG, Carter G. The species dependence of inert gas ion incorporation in the ion-induced deposition of tunsten. Journal of Applied Physics 1999;86(5):2889–2895.

14. Wang J, Saitou T, Sugimoto Y, Wang D, Zhao L, Nakashima H. Effect of Ion Mass and Ion Energy on Low-Temperature Deposition of Polycrystalline-Si Thin Film on SiO_2 Layer. Jpn J Appl Phys 2003;42(Part 2. No. 5B):L511–L513.

15. Bobek T, Facsko S, Kurz H, Dekorsy T, Xu M, Teichert C. Temeral evolution of dot patterns during ion sputtering. Physical Review B 2003;68:085324.

16. Stein DM, McMullan CJ, Li Jiali, Golovchenko JA. A Feeback-Controlled Ion Beam sculpting Apparatus. Review of Scientific Instruments 2004;75:900–905.

17. Ziegler, JF.; Biersack, JP. SRIM-2000 The Stopping and Range of Ions in Matter. 2000. http://www.research.ibm.com/ionbeams/

18. Wittmaack, K. Surface and Depth Analysis Based on Sputtering, in Sputtering by Particale Bombardment III. Behrisch, R.; Wittmaack, K., editors. Springer-Verlag; New York Berlin Heidelberg: 1991. p. 161-246.
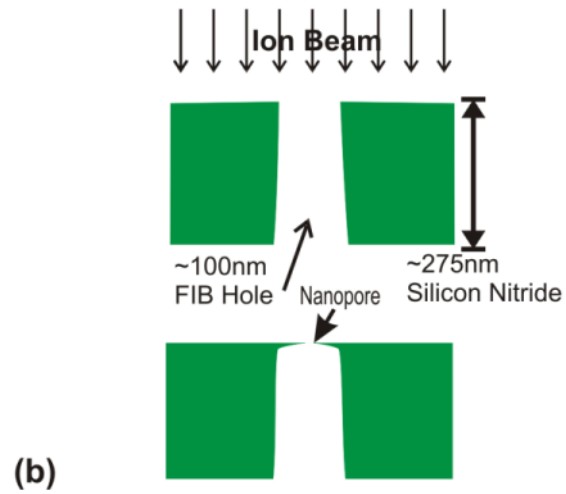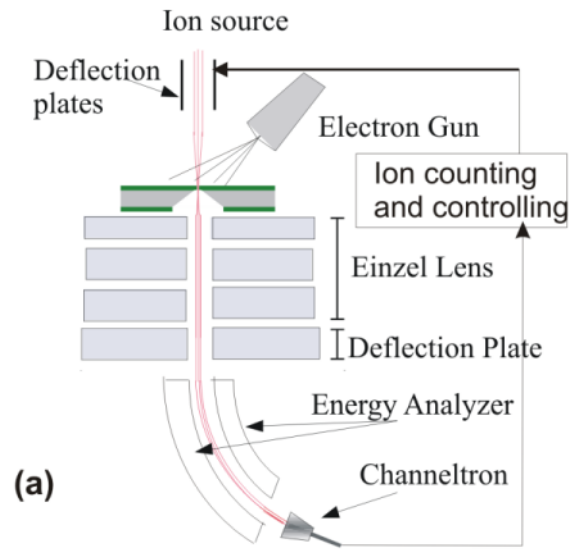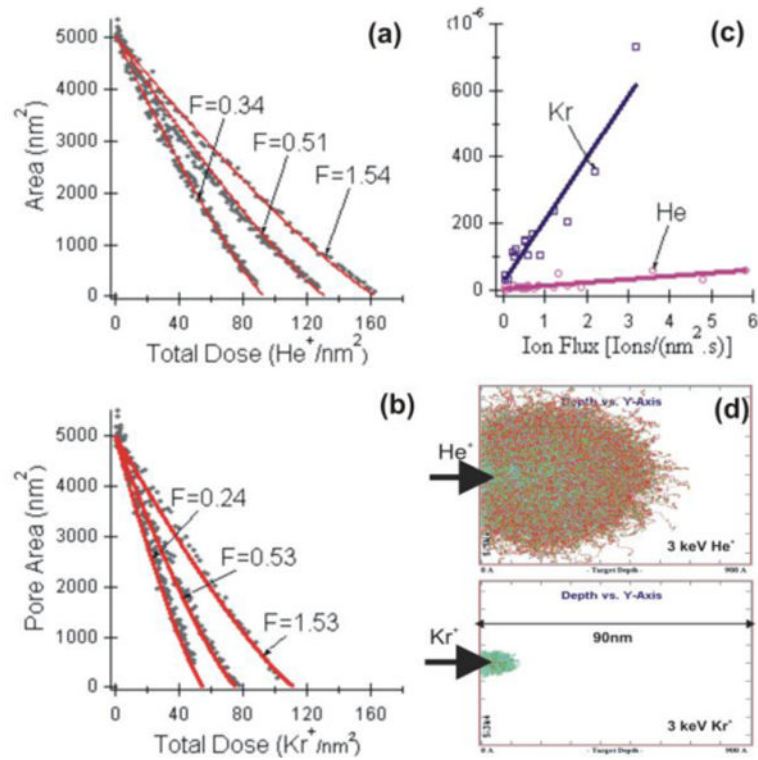
Figure 1.
(**a**) Illustration of ion beam sculpting apparatus. (**b**) Shrinking a larger hole to a smaller one.
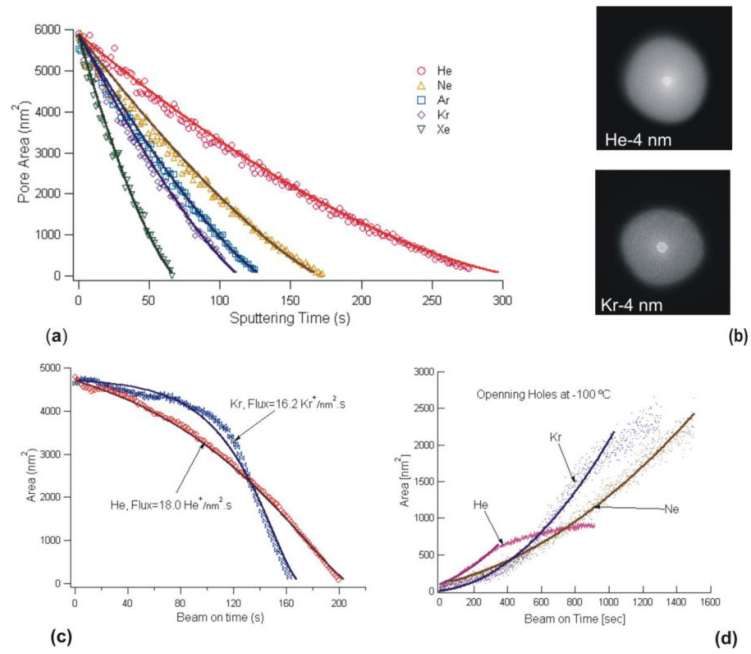
Figure 2.
(**a**) Closing prefabricated FIB holes with He^+, Ne^+, Ar^+, Kr^+, and Xe^+ at low flux 0.5-0.6 Ions/nm^2. The solid lines are fits from Equation 2. (**b**) TEM image of nanopores made by He^+(top) and Kr^+(bottom). (**c**) Ion beam pore closing at high flux: F=18.0 He^+/(nm^2s^2) for He and F=16.2 Kr^+/(nm^2s^2) for Kr. The solid curves are fits to the data to Equation 2. (**d**) Nanometer pores made at 28 °C in Fig.(2a) opened at -100°C with the same ions and flux.

Figure 3.
(**a**) Ion beam flux dependence of pore closing for He, and (**b**) for Kr. (**c**) $(1/X_m)^2$ versus flux obtained by fitting pore closing data to Equation 2. (**d**) SRIM simulation the range of 3 keV He (top) and Kr (bottom) ion beams into silicon nitride. 100,000 ions were used. The stoicheometry of silicon nitride used here is $Si_{3.5}N_4$, and the density was set to 3.1 g/cm^3.
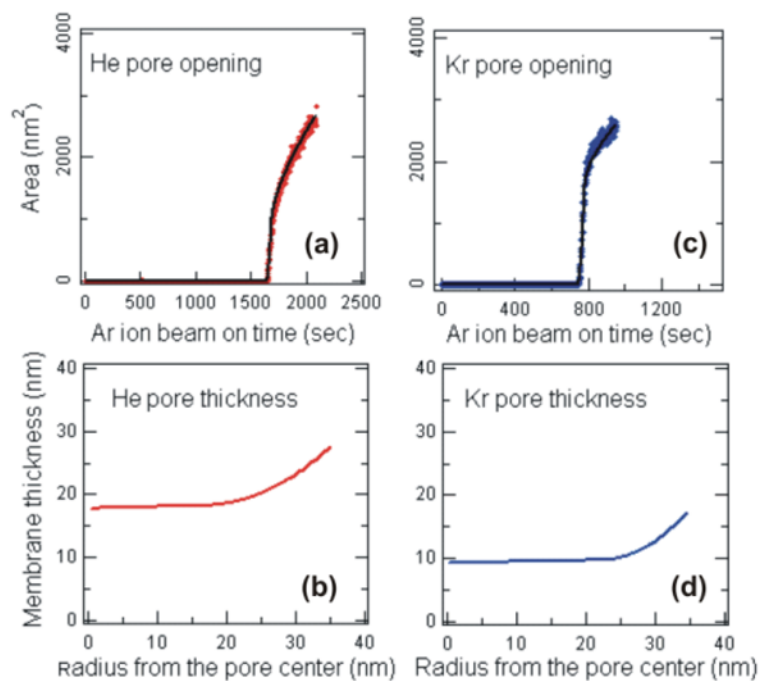
Figure 4.
Thickness profile for He and Xe closed pores. (**a**) A completely He$^+$ closed pore (F=0.58) opened at -100°C with Ar$^+$ at F=0.53. (**b**) The calculated He pore thickness profile for data in 4a. (**c**) A Kr$^+$ completely closed pore (at F=0.53) opened at -100°C with Ar at F=0.61. (**d**) The calculated Kr pore thickness profile for the data in 4c.

Table I

The range and stopping power of 3 keV various noble gases into low stress silicon nitride membrane calculated by SRIM. For this series of calculations, the low stress silicon nitride membrane was given a stoicheometry of $Si_{3.5}N_4$, and the density was set to 3.1 g/cm^3. To calculate the adatom generating yield Ya and sputtering yield Ys from the SRIM program, a surface binding energy of 3.4 eV was used. All values were calculated from the SRIM program except the 5th column: the mean thickness of pores was determined by experiments performed in this work as shown in Fig.4.

Gas	dE/dx (Elec.) (eV/Å)	dE/dx (Nuc) (eV/Å)	The mean Penetration depth (Å)	The mean thickness of pore (Å)	Ys (atom per ion)	Ya atom per ion	S_E nm/ion
He	4.37	2.52	230	196±25	0.23	0.18	11.3±0.4
Ne	5.50	36.9	60	145±25	2.05	1.79	31.1±1.6
Ar	8.31	67.9	45	97±44	2.06	2.31	47.2±1.2
Kr	7.17	100	43	99±9	2.25	2.70	62±5.8
Xe	6.92	110.5	46	78±27	2.21	3.07	52.6±1.8